Experimental and numerical characterization of fatigue crack propagation in high-speed railway wheel ER8 steel

Chaichayo SUETRONG[1], and Vitoon UTHAISANGSUK[1,*]

[1] *Centre for Lightweight Materials, Design and Manufacturing, Department of Mechanical Engineering, Faculty of Engineering, King Mongkut's University of Technology Thonburi, Thailand*

*Corresponding author e-mail: vitoon.uth@kmutt.ac.th

Abstract

In this work, characteristics of fatigue crack growth in the Paris regime of the rail wheel steel grade ER8 were investigated. Experimental crack growth tests under different cyclic loads of a compact tension (CT) specimen and corresponding FE simulations were carried out. The extended FE method (XFEM) coupled with damage evolution based on the strain energy release rate or the Paris law was applied to describe the crack propagation mechanism in the tested CT samples. Hereby, the fatigue fracture model parameters were firstly determined from the experimental data. It was found that the predicted crack growth rates agreed well with the experimentally gathered results. Subsequently, fatigue crack propagations of the investigated wheel steel under varying load levels, load ratios and lengths of pre-crack were studied using the FE approach and the obtained crack growth characteristics were compared and discussed.

1. Introduction

Among several components of the railway vehicle its wheels are one of the most important parts. Because it directly affects the safety of passengers, especially in the case of high-speed railway in which very high driving speeds are concerned. There have been researches with regard to different aspects of failures emerged in railway components [1-6]. In 1998, one of the very serious train accidents occurred in Germany was likely caused by a fatigue crack in only one wheel that finally led to fractures and disasters [1]. In general, the railway wheel grade ER8 specified by EN 13262 has been widely used in many high-speed trains. Such rail wheel steels mainly composed of a mixture of pearlitic and ferritic phases, which was sufficiently strong and showed high toughness [2-6]. Zheng *et al.* [3] developed a wheel steel containing high amounts of Si and Mn and low content of Cr. It was reported that this steel exhibited a good balance of strength and impact toughness as a result of decreased inter-lamellar spacing of pearlite while higher phase fraction of pro-eutectoid ferrite. Fang *et al.* [4] studied fatigue failures of a high speed railway wheel steel at varying temperatures. It was shown that unequal microstructure distributions in the wheel rim and wheel web strongly influenced its fatigue lifetime. Zhang *et al.* [5] also showed that the incompatibility of plastic deformation of observed non-uniform microstructure including bainite promoted the formation of fatigue cracks. With respect to the effects of load types, fatigue limit and respective S-N curves of ER8 wheel steel under tension-shear multiaxial conditions were determined by Zhang *et al.* [6]. It was found that large induced shear stresses could significantly affect the fatigue behaviour and alter the fracture mode. A fatigue crack in railway wheels could be initiated due to some subsurface defects and its growth basically took place under a complex condition. Peixoto *et al.* [2] characterized fatigue crack growth of steel from a Spanish AVE train wheel. The fatigue crack growth rates and propagation direction under different loading modes of compact tension (CT) specimens were measured and compared with the results from FE simulations.

In the recent years, FE simulations have been widely applied to demonstrate different crack developments in alloys under various loading conditions. Mazlan *et al.* [7] performed FE simulations for predicting fatigue life of aluminum sheet grade 2024-T3 at low temperatures, in which yield strength, ultimate strength and S-N curve were used as the material input parameters. Martinez *et al.* [8] investigated fretting fatigue crack propagation of a railway axle subjected to bending load. Hereby, a combined technique of extended finite element method (XFEM) and two fatigue crack growth criteria, namely, maximum tangential stress (MTS) and minimum shear stress range was applied. Bergara *et al.* [9] employed a XFEM-based linear elastic fracture mechanics (LEFM) approach to simulate fatigue crack growth at the side of a rectangular beam subjected to four-point bending. Their experimental and numerical results showed a good agreement. Crack growth and fatigue life of cracked attachment lugs of aluminum grade 7075-T6 were estimated by using XFEM in Naderi *et al.* [10]. Different loading boundary conditions noticeably influenced the calculated life. Vempati *et al.* [11] carried out FE simulations coupled with XFEM to analyse stress distribution and predict fatigue life of Ti-6Al-4V cruciform shape welded joints with different weld geometries. A fatigue crack growth in helical gear tooth root was simulated by using the LEFM-XFEM and its fatigue life was calculated by the Paris equation in Rad *et al.* [12]. A fatigue

life under mixed-mode and constant amplitude condition was predicted by means of the Paris law model in LEFM based FE simulations for two different loading angles in Alshoaibi *et al.* [13]. The determined results were in accordance with the experimental data from the given literatures. Salehnejad *et al.* [14] carried out crack failure analysis on the exhaust manifold of a diesel engine on the basis of the critical fracture toughness (K_{IC}) and FE approach. CT specimens with different notch lengths were firstly tested at a high temperature for determining the critical fracture value of investigated alloy. A numerical calculation of the Paris law constants for a carbon steel was done by using a two-scale model in Mlikota *et al.* [15]. The microstructure-scale FE model coupled with the Tanaka-Mura equation was used to determine the fatigue crack growth rate at a crack tip. Then, the macroscopic model was performed to obtain the stress intensity factor. Then, they further simulated the fatigue crack evolution in the steel [16-18]. The number of cycles for short crack initiation was estimated with regard to stress distribution in the microstructural model, while the LEFM method and Paris law were applied to describe the long crack growth up to final fracture and the corresponding S-N curve. Wei *et al.* [19] analysed the fatigue fracture behaviour of gear teeth using XFEM, in which effects of initial crack geometries and cyclic load factors were considered.

As presented, a more accurate prediction of fatigue crack in railway components is necessary for achieving the reliable rail transportation. In particular, fatigue crack propagation in railway wheel still needed to be investigated more precisely. Therefore, it was aimed in this work to apply FE simulations for describing the fatigue crack development of wheel steel grade ER8 based on the LEFM. The XFEM technique was taken into account for representing the growth mechanisms of fatigue long crack in this wheel material. Tensile tests of sub-size specimens and fatigue crack growth tests of CT specimens were conducted. Obtained stress-strain curves and materials parameters of the Paris law were used for the fatigue fracture analyses in FE simulations. The numerical results were firstly validated with the experimental data. Subsequently, fatigue crack growth in CT samples under different load levels, loading ratios and initial lengths of pre-crack were analysed and compared.

2. Materials

The material used in this work was taken from the railway wheel grade ER8. This grade is commonly used in many high-speed trains. Note that the rim area of wheel was considered here, because it was the wheel section which was subjected to severe loads and was also in a direct contact with the rail. The rim thus required higher strength in comparison with the web. Then, all tested samples were machined from the wheel rim together with the complex surface layer. The chemical composition of examined steel was initially analysed by an optical emission spectrometer (OES). It was found that the results shown in Table 1 was in accordance with the standard of railway wheel grade ER8, which presented a typical medium carbon steel. Then, metallographic sample of the steel was prepared for a microstructure observation, in which the etchant of 2% Nital solution was employed. The microstructure of steel specimen was afterwards revealed by light optical microscope (LOM) and scanning electron microscope (SEM), as depicted in Figure 1(a) and 1(b), respectively. The similar microstructure was found for the whole section of the used wheel rim. It can be seen that the microstructure of grade ER8 wheel steel mainly composed of the pearlitic matrix phase including a little amount of randomly dispersed ferritic phase. The white area was the ferrite, while the brown area was the pearlite. The SEM micrograph showed the lamellar structure of pearlite which was distinguished from the ferritic areas. Such microstructure was also reported in other works [2-5]. This microstructure characteristic could strongly govern the fatigue crack onset and propagation as shown in [5].

Table 1 Chemical composition of the investigated steel grade ER8, mass content in %.

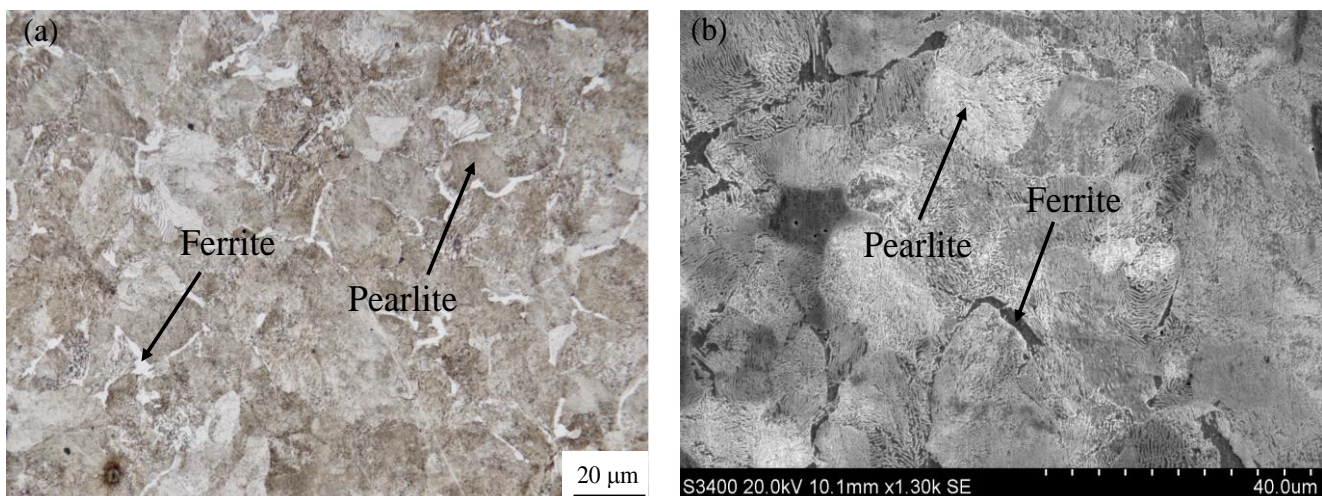| Steel grade	C	Si	Mn	P	S	Cr	Ni	Mo
ER8	0.58	0.22	0.71	0.04	0.04	0.04	0.04	0.007

Figure 1 Microstructure of the investigated ER8 wheel steel by (a) LOM and (b) SEM.

3. Experimental

3.1 Tensile Test

Tensile tests of the investigated steel grade ER8 were performed for determining its mechanical properties. The sub-size tensile specimen was prepared according to the standard ASTM E8. The specimen had a thickness of 2 mm and a gauge length of 25 mm, as illustrated in Figure 2. The tensile tests were conducted on a 50 kN universal testing machine at room temperature with the crosshead speed of 3 mm·min^{-1}. During the test, elongation of the deformed specimen was gathered by a digital image correlation (DIC) technique until fracture. Three repeated tests were done. As a result, stress-strain responses of the steel were determined.

3.2 Fatigue crack growth test

In this work, fatigue crack growth tests were carried out by means of the CT sample, whose geometry is demonstrated in Figure 3(a). This CT specimen was adapted with regard to the ASTM E647 standard for the measurement of fatigue crack growth rate [20]. The notch of specimens was prepared by means of an electro discharge wire cut machine and its orientation was parallel to the tangential direction of the wheel. It was noted that the fatigue load of an actual railway wheel can be more complex so that CT specimen tests under mixed-mode or multi-axial stress state might be required. However, crack growth behavior was often considered under mode I condition or tension stress state as it represented the most severe loading condition [9]. Thus, the CT sample under mode I was examined here. The cyclic crack growth tests were performed on the Zwick Roell 250 kN universal testing machine at room temperature. A sinusoidal wave of the stress ratio of 0.1 ($R = 0.1$) at the frequency of 10 Hz was employed. A 30 mm gauge length extensometer was applied on the CT specimens for gathering the growth speed of fatigue crack along with the number of cycles. Furthermore, the initial pre-crack with the size of 1.5 mm was generated before the crack propagation tests by using the maximum load of 6 kN and the same stress ratio. Note that the ASTM E647 standard recommended the minimum size of pre-crack of at least 1 mm.

Basically, fatigue crack growth behavior of steel under a specified cyclic load could be divided into three regions. The region I exhibited a propagation of short crack with a very low rate, in which the corresponding crack length was too small for capturing by a conventional method. Then, the crack growth rates in the II region, known as the Paris region, were typically in the order of 10^{-9} m/cycle to 10^{-6} m/cycle. The growth rate increased linearly in this region. The Paris law was commonly used to represent a fatigue crack growth rate in this region, which is played a significant role on the fatigue life of material. The Paris law showed the relationship between the fatigue crack growth rate (da/dN) and stress intensity factor range (ΔK) of material under cyclic load, as expressed in Equation (1).

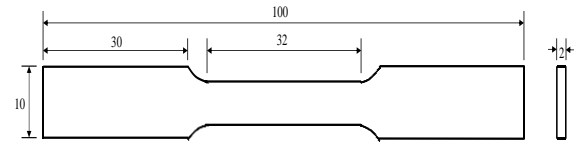$$da/dN = C \cdot (\Delta K)^m \qquad (1)$$

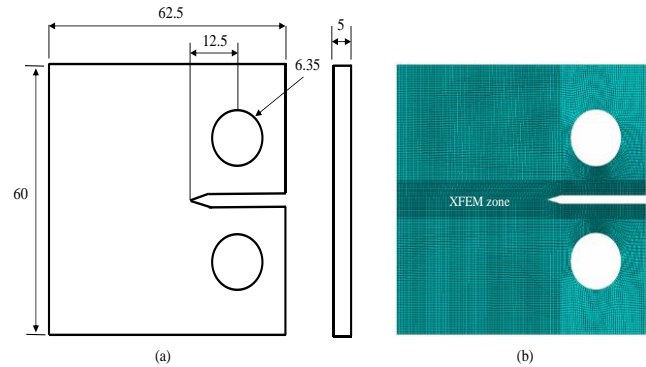**Figure 2.** Geometry of the used sub-size tensile specimen.

Figure 3. (a) Geometry and (b) FE model of the used CT specimen for fatigue crack growth test.

The Paris constants C and m were the materials parameters which depended on various influencing factors such as temperature, test environment, specimen geometry and loading ratio. During the tests, fatigue crack length (a) was obtained as a function of the increasing number of cycles (N) and the stress intensity factor range (ΔK) was simultaneously determined. The calculation was done based on the LEFM approach and an initial fatigue crack was present. From these cyclic crack growth rate data, the material constants C and m of the investigated steel could be directly obtained. The Paris equation can be then applied to study fracture growth patterns and estimate remaining life of crack-afflicted component. In this work, two different maximum loads of 4 kN and 5 kN were applied and the results served for validating the derived material constants.

4. FE modelling

FE simulations of fatigue crack propagations in the CT specimens were conducted. Figure 4 depicts the FE model and mesh discretization of the sample. The 2D model corresponded to the geometry of CT sample in Figure 3(b). The frequency and initial length of pre-crack was also defined as in the experiments. The 4 nodes quadratic plane strain elements and irregular mesh size were used. A pin constraint was employed as rigid body at both specimen holes. A vertical cyclic load was defined at the upper pin, while all motions of the bottom pin were hindered. The XFEM was defined to the expected crack propagation zone in the center of the specimen. Hereby, the maximum principal stress for the initial crack criterion was given in the traction separation law of the XFEM. True stress-true strain curve from the tensile test was used to define the elastic-plastic properties of material. In addition, fatigue crack parameters determined from the fatigue crack growth test were applied. The mesh sensitivity was also first studied.
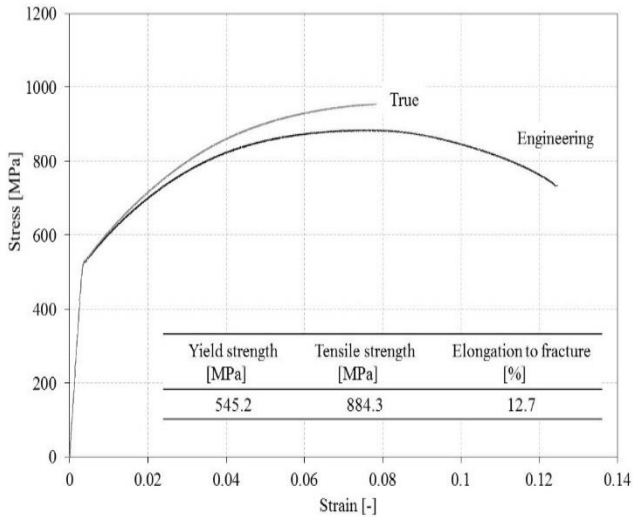
Figure 4. Determined stress-strain curves and tensile properties of the ER8 wheel steel.

5. Results and discussion

5.1 Experimental results

The engineering and true stress-strain curves of the examined wheel steel grade ER8 were determined from the tensile test, as illustrated in Figure 4. It is seen that the steel exhibited relatively high strengths but moderate elongation. The yield strength, tensile strength and elongation at fracture of the ER8 steel are also provided. It is noticed that the strength properties were somewhat higher than those of the pearlite/ferrite wheel steel in [2]. This was likely attributed by the higher carbon content of 0.58 wt% compared to 0.49 wt% in that study. Nevertheless, the tensile test results were very similar to those reported in [5], since the microstructures of both steels showed the similar phase fractions of ferrite and pearlite. Moreover, the steel exhibited rather high post-uniform elongation or toughness characteristic. The true stress-strain curve was given for the crack growth simulations and the tensile strength was then applied as the crack onset criterion of the traction separation law.

The propagation of fatigue crack was largely dependent on the applied load and the number of cycles. By the XFEM or the virtual crack closure technique (VCCT), predicted crack growth behaviour was governed by the Paris law, in which the range of energy release rate (ΔG) at the crack tip was taken into account. This ΔG range was characterized by the difference between G_{max} and G_{min}, which were the energy discharge rates that occurs when a crack-afflicted structure was loaded to the maximum and minimum load P_{max} and P_{min}, respectively. The relationship between the energy release rate G and the stress intensity factor K is provided as shown in Equation (2).

$$G_I = \frac{K_I^2}{E} \qquad (2)$$

The G_I is the fracture energy release rate under mode I and E is the elastic modulus. The Paris law in the fatigue crack simulations was defined as the relationship between the crack growth rate (da/dN) and the range of fracture energy release rate (ΔG).

From the fatigue test, developed crack lengths and number of cycles were gathered for two maximum loads at the constant R ratio of 0.1. Figure 5(a) presents the resulted fatigue crack propagation rates in term of crack length and number of cycles. The 4 kN load required approximately 142,000 cycles for achieving an unstable crack growth. By increasing the maximum fatigue load of 25%, crack growth was noticeably accelerated, in which the CT sample subjected to 5 kN load just reached about 128,000 cycles. In addition, from the relationship between fatigue crack growth rate (da/dN) and stress intensity factor range (ΔK), as depicted in Figure 5(b), the material constants C and m of the Paris equation could be obtained. Hereby, the wheel steel grade ER8 exhibited the Paris constants C and m of 4.27E-9 and 3.27, respectively for the load ratio of 0.1. Note that for metals the typical value of the exponent m was between 2 and 4 [15]. It was found that this steel grade showed the fatigue crack propagation in the ΔK range of 20 MPa·m$^{1/2}$ to 55 MPa·m$^{1/2}$ by the given load ratio. The determined crack growth parameters C and m were slightly higher than those of the wheel steel with a fully pearlitic structure investigated in [2].
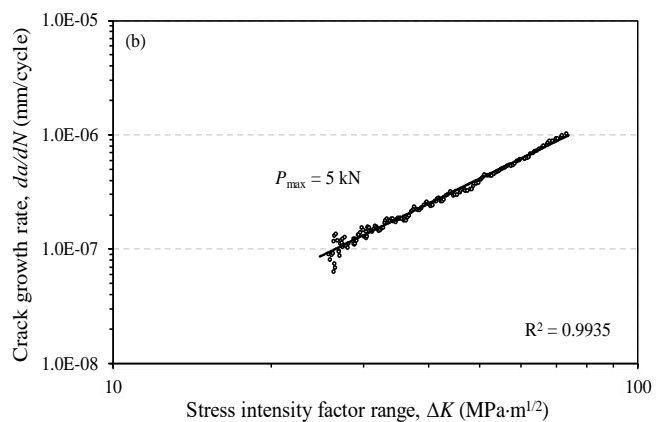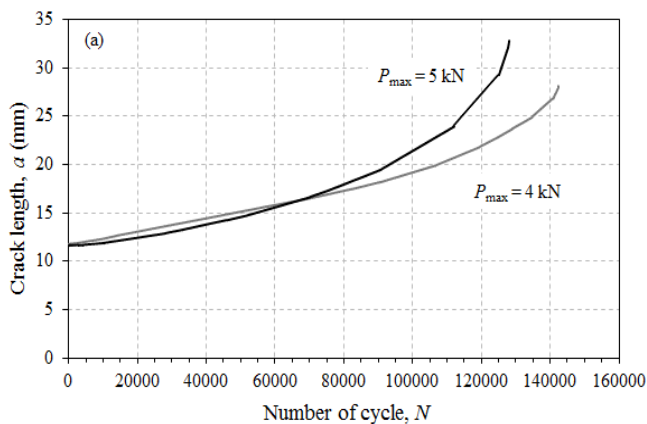

Figure 5. Results of fatigue crack growth tests: (a) crack length vs. number of cycle and (b) crack growth rate vs. stress intensity factor range.

5.2 FE results and validations

The fatigue crack growth behavior of wheel steel was examined by FE simulations of CT specimen employing XFEM. The developed crack length during continuously increasing number of loading cycles were predicted with regard to the Paris law, in which all parameters were obtained from the experiments. Firstly, a study of mesh convergence of the crack propagation simulation was performed. The crack lengths determined from the simulations using different mesh sizes at the same crack length before final fracture as observed in the experiment are demonstrated in Figure 6. It is seen that the simulations achieved a convergence at when the number of element larger than around 10000 elements. Therefore, in this work, the minimum mesh size of 0.25 mm and number of element of about 20000 were used. Subsequently, increased crack lengths against number of cycles of the given cyclic loads were determined from the simulations.

The predicted crack propagation rates are compared with the correspondingly experimental results for the maximum fatigue loads of 4 kN and 5 kN in Figure 7(a) and 7(b), respectively. Obviously, the crack growth mechanisms of the steel grade ER8 could be well described by the FE simulations coupled with XFEM and Paris law. The averaged deviations of the numerical predictions were about 11% and 5.2% in the case of 4 kN and 5 kN, respectively.

Afterwards, effects of fatigue load characteristic on the crack propagation were further investigated by the proposed FE simulations of CT specimen. The maximum cyclic load was varied between 3 kN and 9 kN. The frequency, load ratio and other boundary conditions remained unchanged. Figure 8(a) depicts the calculated crack length vs. number of cycle curves for different maximum loads. It was found that by increasing the magnitude of cyclic load fatigue crack growth rates became considerably higher. In order to attain a crack length of 25 mm, which was approximately the critical crack length before rapid crack as observed in the experiment, the lower fatigue load than 4.5 kN larger than 105 cycles was needed. In contrast, with the loads higher than 6 kN the number of cycle to fracture was reduced more than 5 times. At the maximum load of 9 kN, the crack propagation became very high. Moreover, FE simulations of CT specimens for varying load ratios between 0.1 and 0.7 combined with the same maximum load of 4.5 kN were performed. From the results, as shown

in Figure 8(b), it is seen that increasing the load ratio led to lower crack growth rate. In the case of load ratio of 0.9, an obvious crack propagation occurred first when the number of cycle was higher than 106. The alteration of the magnitude of fatigue load exhibited more significant effects on the crack growth rather than that of the load ratio.

The effects of pre-crack on the crack propagation behavior were also examined. FE simulations of CT specimens including different lengths of the pre-crack between 1.5 mm and 10 mm were conducted. The determined numbers of cycles to the critical crack length are presented for the varying pre-cracks in Figure 9(a). Note that the critical crack length of 25 mm as observed in the experiment was used as the reference. The maximum load of 4.5 kN and load ratio of 0.1 were applied for all cases. The results showed that with longer initial pre-crack the number of cycles to the critical crack length continuously decreased. In addition, the average fatigue crack growth rates of the CT samples afflicted with different pre-cracks were gathered, as illustrated in Figure 9(b). The crack propagation rate was considerably increased as the pre-crack became larger than about 7.5 mm. Hereby, the fatigue crack growth likely continued into the region III where rapid crack and unstable fracture occurred. Hereby, the fatigue crack growth likely continued into the region III where rapid crack and unstable fracture occurred. It is noted that FE simulation based on the LEFM and Paris equation was limited to the region II of the stable fatigue crack growth. The defined pre-crack length
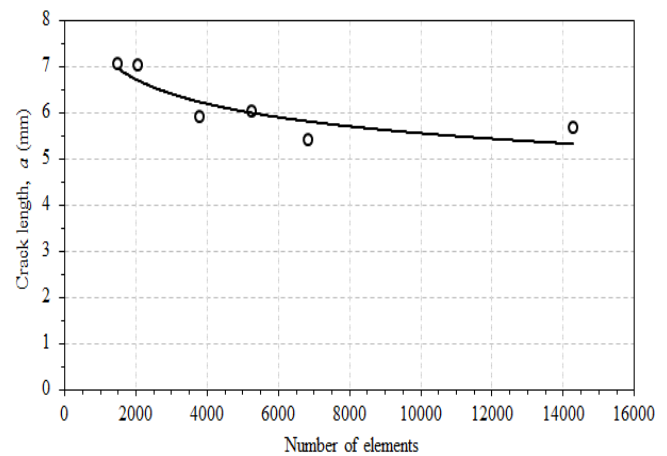

Figure 6. Mesh dependency of fatigue crack growth simulation using XFEM.
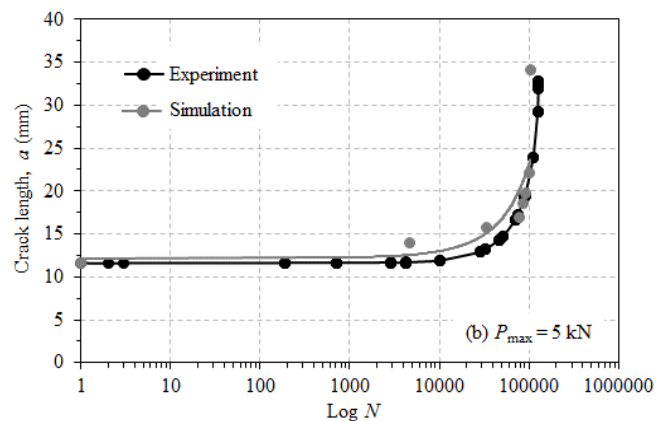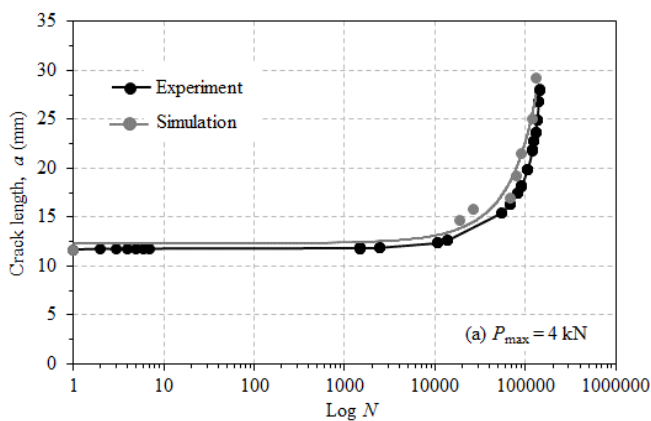

Figure 7. Comparisons between experimental and predicted crack length vs. load cycle curve for the maximum load of (a) 4 kN and (b) 5 kN.

and correct material constants of the Paris law were the most important factors for ensuring the prediction accuracy of the crack growth behaviour by FE simulations using XFEM. The growth of a fatigue short crack was governed by the microstructure of concerned steel. On the other hand, for the propagation of fatigue long crack, the stress intensity.

Finally, Figure 10 demonstrates the crack propagation paths observed in the experiments and simulations in comparison using

the same initial crack length and load conditions. Two stages of crack development, namely, at the onset of fatigue crack growth and before final rapture were shown. It is seen that the crack propagation characteristic in the experiment was well in accordance with that predicted by the FE simulation. Furthermore, from the simulations, equivalent stress distribution around the crack tip could be also provided.
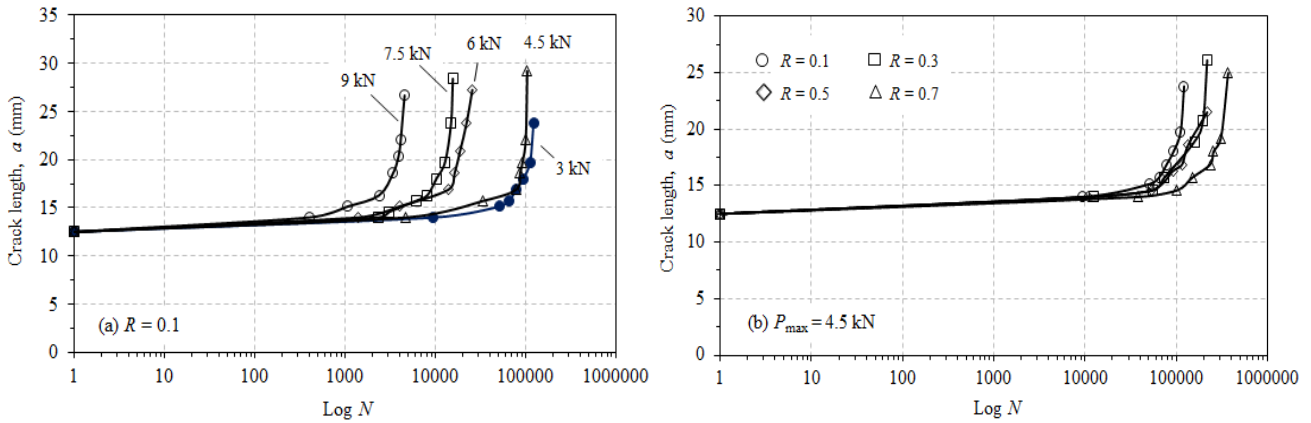

Figure 8. Predicted fatigue crack length vs. load cycle for different (a) magnitudes of cyclic loading ($R = 0.1$) and (b) load ratios ($P_{max} = 4.5$ kN).
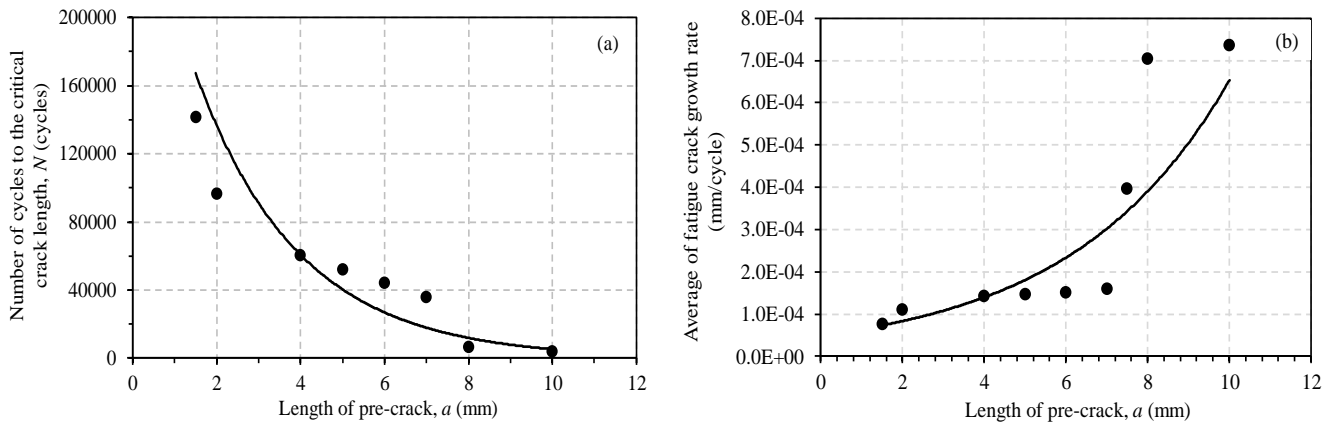

Figure 9. Influences of pre-crack: (a) number of cycles to critical crack length and (b) crack growth rate vs. length of pre-crack.
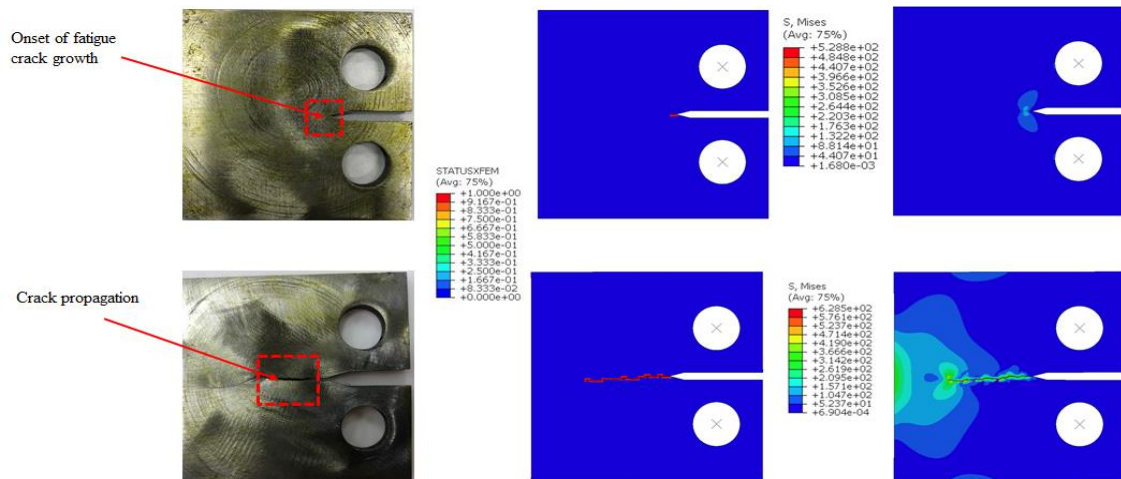

Figure 10. Comparisons of crack developments observed in the experiment and predicted by FE simulation using XFEM.

6. Conclusions

The fatigue crack growth behaviour of the grade ER8 railway wheel steel was investigated. The wheel steel exhibited high strength and moderate elongation and its microstructure mainly contained pearlitic matrix dispersed with small amount of ferritic phase. FE simulations coupled with XFEM and Paris law of CT specimens were performed for describing occurred fatigue crack propagation. The Paris material constants of the examined steel were directly obtained from the experiment. The stress-strain curves and determined materials parameters were given. It was found that the simulations could well predict the crack propagation mechanisms at different applied loads in term of increased crack length vs. number of cycles as well as respective crack path. In addition, the effect of the magnitude of cyclic load on the crack growth rate were more noticeable than that of the load ratio. The pre-crack length strongly governed the number of cycle to the critical crack length. When the pre-crack was larger than a certain length the crack growth rate was increased into the region of unstable rapid crack where the application of FE simulation using XFEM based on LEFM was limited.

Acknowledgements

References

[1] V. Esslinger, R. Kieselbach, R. Koller, and B. Weisse, "The railway accident of Eschede –Technical background," *Engineering Failure Analysis,* vol. 11, no. 4, pp. 515-535, 2004.

[2] D. F. C. Peixoto, and P. M. S. T. de Castro, "Fatigue crack growth of a railway wheel," *Engineering Failure Analysis,* vol. 82, pp. 420–434, 2017.

[3] D. F. Zeng, L. T. Lu, Y. H. Gong, N. Zhang, and Y. B. Gong, "Optimization of strength and toughness of railway wheel steel by alloy design," *Material and Design*, vol. 92, pp. 998-1006, 2016.

[4] X. Y. Fang, Y. X. Zhao, and H. W. Liu, "Study on fatigue failure mechanism at various temperatures of a high-speed railway wheel steel," *Materials Science and Engineering A,* vol. 696, pp. 299-314, 2017.

[5] G. Z. Zhang, C. P. Liu, R. M. Ren, S. Wu, H. X. Yin, T. Cong, and X. Li, "Effect of non-uniform microstructure on wear property of ER8 wheel steel," *Wear*, vol. 458-459, 203416, 2020.

[6] Q. S. Zhang, I. Toda-Caraballo, Q. Li, J. C. Han, J. Han, J. W. Zhao, and G. Z. Dai, "Tension-shear multiaxial fatigue damage behavior of high-speed railway wheel rim steel," *International Journal of Fatigue,* vol. 133, 105416, 2020.

[7] S. Mazlan, N. Yidris, R. Zahari, E. Gires, D. L. A. Majid, and K. A. Ahmad, "Prediction of fatigue life of aluminum 2024-T3 at low temperature by finite element analysis," *Journal of Mechanical Engineering Science,* vol. 14, no. 3, pp. 7170-7180, 2020.

[8] J. C. Martínez, L. V. V. Useche, and M. A. Wahab, "Numerical prediction of fretting fatigue crack trajectory in a railway axle using XFEM," *International Journal of Fatigue*, vol. 100, pp. 32-49, 2017.

[9] A. Bergara, J. I. Dorado, A. Martín-Meizoso, and J. M. Martínez-Esnaola, "Fatigue crack propagation in complex stress fields: experiments and numerical simulations using the extended finite element method (XFEM)," *International Journal of Fatigue*, vol. 103, pp. 112-121, 2017..

[10] M. Naderi, and N. Iyyer, "Fatigue life prediction of cracked attachment lugs using XFEM," *International Journal of Fatigue,* vol. 77, pp. 186-193, 2015.

[11] S. R. Vempati, K. B. Raju, and K. V. Subbaiah, "Simulation of Ti-6Al-4V cruciform welded joints subjected to fatigue load using XFEM," *Journal of Mechanical Engineering Science,* vol. 13, no. 3, pp. 5371-5389, 2019.

[12] A. A. Rad, M. R. Forouzan, and A. S. Dolatabadi, "Three-dimensional fatigue crack growth modelling in a helical gear using extended finite element method," *Fatigue and Fracture Engineering Materials Structure,* vol. 37, pp. 581-591, 2014.

[13] A. M. Alshoaibi, and Y. A. Fageehi, "2D finite element simulation of mixed mode fatigue crack propagation for CTS specimen," *Journal of Materials Research Technology,* vol. 9, no. 4, pp. 7850-7861, 2020.

[14] M. A. Salehnejad, A. Mohammadi, M. Rezaei, and H. Ahangari, "Cracking failure analysis of an engine exhaust manifold at high temperatures based on critical fracture toughness and FE simulation approach," *Engineering Fracture Mechanics*, vol. 211, pp. 125-136, 2019.

[15] M. Mlikota, S. Staib, S. Schmauder, and Z. Božić, "Numerical determination of Paris law constants for carbon steel using a two-scale model," *Journal of Physics: Conference Series,* vol. 843, pp. 012042, 2017.

[16] M. Mlikota, S. Schmauder, and Z. Božić, "Calculation of the Woehler (S-N) curve using a two-scale model," *International Journal of Fatigue*, vol. 114, pp. 289-297, 2018.

[17] V. K. Goyal, and R. Jorge, "Micro-scale crack propagation using the eXtended finite element method," in *Proceedings of the 57th AIAA/ASCE/AHS/ASC Structures, Structural Dynamics, and Materials Conference.* San Diego, California, USA: 4-8 January 2016.

[18] R. Dekker, F. P. Van der Meer, J. Maljaars, and L. J. Sluys, "A cohesive XFEM model for simulating fatigue crack growth under mixed-mode loading and overloading," *International Journal of Numerical Methods Engineering,* vol. 118, pp. 561-577, 2019.

[19] Y. Wei, and Y. Jiang, "Fatigue fracture analysis of gear teeth using XFEM," *Transactions of Nonferrous Metals Society of China,* vol. 29, no. 10, pp. 2099-2108, 2019.

[20] ASTM, Standard test method for measurement of fatigue crack growth rates, E647, *American Society for Testing and Materials (2008).*

[21] A. Negi, G. Bhaedwaj, J. S. Saini, and N. Grover, "Crack growth analysis of carbon nanotube reinforced polymer nano-composite using extended finite element method," *Journal of Mechanical Engineering Science,* pp. 1-21, 2021.